Probing two Universal Extra Dimension model with leptons and photons at the LHC and ILC

Kirtiman Ghosh[a]
Department of Physics, University of Calcutta,
92, A. P. C. Road, Kolkata 700009, India.

ABSTRACT

We discuss the collider signatures of electroweak $(1,0)$-mode excitations in the framework of two universal extra dimension (2UED) at the LHC and ILC. In general, pair production of electroweak $(1,0)$-mode particles of 2UED gives rise to *multi lepton plus missing transverse momentum* signal. Upto $1/\mathrm{R} = 400$ GeV *2-lepton plus missing transverse momentum* signal and upto $1/\mathrm{R} = 600$ GeV *3-lepton plus missing transverse momentum* signal stands over the 5σ standard deviation of the Standard Model background at the LHC with 100 fb^{-1} integrated luminosity. At ILC we study *single photon plus missing energy* signal from the production of $U(1)$ gauge boson in association with a $U(1)$ spinless adjoint. With proper choice of beam polarization, signal strength is greater than 5σ standard deviation of the Standard Model background almost upto the kinematic limit of the collider.

1 Introduction

One of the goals for the future collider experiments will be to find out whether a new dynamics beyond the Standard Model (SM) really exists around the TeV scale of energy. A great effort have been also put in to pin down the exact nature of this new dynamics. In this endeavor, supersymmetry and models with one or more *extra dimension* play very special role.

Extra dimensional theories can be classified into several classes. Models of ADD [1] or RS [2] have been proposed to circumvent the long-standing hierarchy problem. In this framework, gravity lives in $(4 + D)$ dimensions and the SM particles are confined to a 3-brane (a $(3 + 1)$ dimensional space) embedded in the $(4 + D)$ dimensional bulk, with D spatial dimensions compactified on a volume V. For large enough value of this extra dimensional volume V, the fundamental $4 + D$ dimensional Plank mass can be as low as 1 TeV, although the effective 4 dimensional Plank mass can be as large as 10^{19} GeV. There are some interesting generalization of these models in which the SM particles are confined to a $(3+n)$-brane ($3+n+1$ dimensional manifold) embedded in a $(4+D)$ dimensional bulk [3]. Since n spatial dimensions are compact, in this framework, effective 4-dimensional theory also contain the Kaluza-Klein (KK) excitations of SM fields. The phenomenology of these

[a]E-mail address: kirtiman.ghosh@saha.ac.in

models are extensively studied in Ref. [4]. The volume of n spatial dimensions (internal to the bulk) can not be too large due to the experimental lower bound on the KK-mode masses. There are also models in which the SM particles are confined to a 3-brane which is "fat" i.e. it has an extension in the $(4 + D)$ dimensional bulk [5].

On the other hand, there are class of models where some or all of the SM fields can access the full space-time manifold. One such example is Universal Extra Dimension (UED), where all the fields can propagate in the full manifold [6]. Apart from the rich phenomenology, UED models in general offer possible unification of the gauge couplings at a relatively low scale of energy, not far beyond the reach of the next generation colliders [7]. Moreover, particle spectra of UED models naturally contain a weakly interacting stable massive particle, which can be a good candidate for cold dark matter [8, 9].

A particular variant of the UED model where all the SM fields propagate in $(5 + 1)$ dimensional space-time, namely the *two Universal Extra Dimension* (2UED) model has some attractive features. 2UED model can naturally explain the long life time for proton decay [10] and more interestingly it predicts that the number of fermion generations should be an integral multiple of three [11]. When the $(5 + 1)$ dimensional theory is compactified into a $(3 + 1)$ dimensional effective theory, each 6D field decomposes to a tower (known as KK-tower) of 4D fields. Each field in the KK-tower is characterized by a pair of integers (j, k), known as KK-numbers. The zero mode (with $j = k = 0$) fields are identified with the SM particles. In this article we will concentrate on the phenomenology of the $(1, 0)$-mode (the lightest KK-mode) particles.

Recently, signals of 2UED model in future colliders like LHC [13, 14, 15] and ILC [16, 17] have been studied in some details. The pair production of strongly interacting $(1, 0)$ modes at the LHC was previously discussed in Ref. [13]. The production of strongly interacting $(1, 0)$ modes results into *multi lepton + multi jet + missing transverse momentum* signal. It is needless to mention that production rate for strongly interacting particles are high. However, detecting *multi lepton + missing transverse momentum* signal in presence of more than one jets could be challenging. At the same time it is also important to look for other smoking gun signature of this model in other channels and correlating it with the signal from strong production channel. Therefore, in this article we concentrate on the hadronically quiet[2] signals which can arise from the pair production of the $(1, 0)$-mode electroweak particles. We show that the pair production of weakly interacting $(1, 0)$-modes of 2UED at the LHC gives rise to *multi lepton + missing transverse momentum* ($\not{p}_T$) signal. We concentrate only on *2 (3)-lepton +* $\not{p}_T$ signal. The hypercharge gauge boson $B_\mu^{(1,0)}$ decays to $B_H^{(1,0)}$ and a *photon*. The production of $B_\mu^{(1,0)}$ in association with $B_H^{(1,0)}$ can give rise to $\gamma E\!\!\!/$ signal at the LHC. This is a very characteristic feature of 2UED. However, $B_\mu^{(1,0)}$ and $B_H^{(1,0)}$ coupling to quarks, being proportional to the quark hypercharge, $B_H^{(1,0)} B_\mu^{(1,0)}$ production rate is suppressed at the LHC. Consequently, we investigate $\gamma + \not{E}$ signal from $B_H^{(1,0)} B_\mu^{(1,0)}$ production in the context of future e^+e^- collider.

The plan of the article is the following. We will give a brief description of the model in the next section. Signature of $(1, 0)$-mode electroweak particles at the LHC and ILC will be

[2]In an environment like LHC, even a hadronically quiet process, like the one of our interest, is always associated with one or more soft jets due to initial state radiation. Thus in such an environment, one should ask for the absence of any hard jets (say within $p_T > 30$ GeV). An event generator like PYTHIA can easily generate such events with soft jets even the hard partonic process does not have any partons in the final state. In our analysis which is done only at partonic level, we could not implement this.

discussed in section 3 and section 4 respectively. We summarize in the last section.

2 Two Universal Extra Dimensions

In 2UED all the SM fields can propagate universally in the $(5+1)$ dimensional space-time. Four space time dimensions with coordinates x^μ ($\mu = 0, 1, 2, 3$) form the Minkowski space. Two extra spacial dimensions (x^4 and x^5) are flat and are compactified with $0 \leq\ x^4,\ x^5\ \leq L$. This implies that the extra dimensional space (before compactification) is a square[3] with sides L. Identifying the opposite sides of the square will make the compactified manifold a torus. However, toroidal compactification, leads to 4D fermions that are vector-like with respect to any gauge symmetry. The alternative is to identify two pairs of adjacent sides of the square:

$$(y, 0)\ \equiv\ (0, y), \quad (y, L)\ \equiv\ (L, y), \quad \forall\ y \in\ [0, L] \tag{1}$$

This is equivalent to folding the square along a diagonal and gluing the boundaries. Above compactification mechanism automatically leaves at most a single 4D fermion of definite chirality as the zero mode of any chiral 6D fermion [12]. The physics at identified points is identical if the Lagrangian takes the same value for any field configuration:

$$\mathcal{L}|_{x^\mu,y,0}\ =\ \mathcal{L}|_{x^\mu,0,y};\ \ \mathcal{L}|_{x^\mu,y,L}\ =\ \mathcal{L}|_{x^\mu,L,y}$$

This requirement fixes the boundary conditions for 6D scalar fields $\Phi(x^\alpha)$ and 6D Weyl fermions $\Psi_\pm(x^\alpha)$. The requirement that the boundary conditions for 6D scalar or fermionic fields are compatible with the gauge symmetry, also fixes the boundary conditions for 6D gauge fields. The folding boundary conditions do not depend on continuous parameters, rather there are only eight self-consistent choices out of which one particular choice leads to zero mode fermions after compactification. Any 6D field (fermion/gauge or scalar) $\Phi(x^\mu, x^4, x^5)$ can be decomposed as:

$$\Phi(x^\mu, x^4, x^5)\ =\ \frac{1}{L}\sum_{j,k} f_n^{(j,k)}(x^4, x^5)\Phi^{(j,k)}(x^\mu) \tag{2}$$

Where,

$$f_n^{(j,k)}(x^4, x^5)\ =\ \frac{1}{1\ +\ \delta_{j,0}\delta_{k,0}}\left[e^{-in\pi/2}cos\left(\frac{jx^4 + kx^5}{R}\ +\ \frac{n\pi}{2}\right)\ +\ cos\left(\frac{kx^4 - jx^5}{R}\ +\ \frac{n\pi}{2}\right)\right] \tag{3}$$

The compactification radius R is related to the size, L, of the compactified space as : $L = \pi R$. Where 4D fields $\Phi^{(j,k)}(x^\mu)$ are the (j, k)-th KK-modes of the 6D field $\Phi(x^\alpha)$ and n is a integer whose value is restricted to $0, 1, 2$ or 3 by the boundary conditions. Since $f_n^{(j,k)}(x^4, x^5)$ should form a complete set on the compactified manifold, it must satisfy the following:

$$\frac{1}{L^2}\sum_{j,k}\left[f_n^{(j,k)}(x^4, x^5)\right]^*\ f_n^{(j,k)}(x'^4, x'^5)\ =\ \delta(x'^4 - x^4)\delta(x'^5 - x^5) \tag{4}$$

[3]This implies that the size of the two extra dimensions are same. However, the most general 2UED model should include two different sizes for two compactified dimensions instead of one. In the absence of any obvious symmetry that can relate these two length-scales, we are thus considering only a specific choice of parameters of this theory.

The allowed values of j and k should be chosen such that the completeness condition in Eq. 4 is satisfied. It is clear from the form of $f_n^{(j,k)}$ that the functions $f_n^{(1,0)}$ and $f_n^{(0,1)}$ are not independent ($f_n^{(0,1)} = (-1)^n f_n^{(1,0)}$). Therefore, it is sufficient to take $j > 0,\ k \geq 0$ and $j = k = 0$ to form a complete set of functions on the chiral square. It is also obvious from the form of $f_n^{(j,k)}(x^4, x^5)$ that only $n = 0$ allows zero mode ($j = k = 0$) fields in the 4D effective theory. The zero mode fields and the interactions among zero modes can be identified with the SM.

In 6D, the Clifford algebra is generated by six anticommuting matrices: $\Gamma^\alpha,\ \alpha = 0, 1, .., 5$. The minimum dimensionality of Γ matrices in 6D is 8×8. The spinor representation of the $SO(1,5)$ Lorentz symmetry is reducible and contain two irreducible Weyl representation characterized by different eigenvalues of the 6D chirality operator: $\bar{\Gamma} = \Gamma^0\Gamma^1\Gamma^2\Gamma^3\Gamma^4\Gamma^5$. The chirality projection operator is defined as: $P_\pm = (1 \pm \bar{\Gamma})/2$, where $+$ and $-$ label the 6D chiralities defined by the eigenvalues of $\bar{\Gamma}$.

$$\Psi_\pm(x^\alpha) = P_\pm \Psi(x^\alpha); \qquad \bar{\Gamma}\Psi_\pm(x^\alpha) = \pm\Psi_\pm(x^\alpha). \tag{5}$$

The chiral fermions in 6D have four components. Each 6D chiral fermion contains both the chiralities of $SO(1,3)$.

Now we move on to the Standard Model in 6-dimensions. In 6D, the fields and boundary conditions are chosen such that upon compactification, the zero modes of the resulting effective theory should reproduce the SM. The requirements of anomaly cancellation and fermion mass generation force the weak-doublet fermions to have opposite *6D chiralities* with respect to the weak-singlet fermions. So the quarks of one generation are given by $Q_+ \equiv (U_+, D_+),\ U_-,\ D_-$. Since observed quarks and leptons have definite 4D chirality, an immediate constraint is imposed on the boundary conditions of doublet and singlet fermions. The 6D doublet quarks and leptons decompose into a tower of heavy vector-like 4D fermion doublets with left-handed zero mode doublets. Similarly each 6D singlet quark and lepton decompose into the towers of heavy 4D vector-like singlet fermions along with zero mode right-handed singlets. These zero mode fields are identified with the SM fermions. As for example, SM doublet and singlets of 1st generation quarks are given by $(u_L, d_L) \equiv Q_{+L}^{(0,0)}(x^\mu)$, $u_R \equiv U_{-R}^{(0,0)}(x^\mu)$ and $d_R \equiv D_{-R}^{(0,0)}(x^\mu)$.

In 6D, each of the gauge fields, has six components. Upon compactification, they decompose into towers of 4D spin-1 fields, a tower of spin-0 fields which are eaten by heavy spin-1 fields. Another tower of 4D spin-0 fields, all belonging to the adjoint representation of the corresponding gauge group, remain in the physical spectrum. These are the physical *spinless adjoints*. The 6D gluon fields, G_α^a decompose into a tower of 4D spin-1 fields, $G_\mu^{a(j,k)}$, and a tower of spin-0 fields, $G_H^{a(j,k)}$. $G_\mu^{a(j,k)}$ tower includes a zero mode which can be identified with the SM gluons. Similarly 6D $SU(2)$ gauge fields have KK-modes $W_\mu^{(j,k)\pm}$, $W_H^{(j,k)\pm}$, $W_\mu^{(j,k)3}$ and $W_H^{(j,k)3}$, while the hypercharge gauge field has KK-mode $B_\mu^{(j,k)}$ and $B_H^{(j,k)}$. The zero modes of $W_\mu^{(j,k)\pm}$ towers are identified with the SM $W_\mu^\pm$ bosons. The mixing of $W_\mu^{(0,0)3}$ and $B_\mu^{(0,0)}$ gives photon and Z-boson. However, for non-zero modes this mixing is negligible.

The tree-level masses for (j,k)-th KK-mode particles are given by $\sqrt{M_{j,k}^2 + m_0^2}$, where $M_{j,k} = \sqrt{j^2 + k^2}/R$. m_0 is the mass of the corresponding zero mode particle. As a result, the tree-level masses are approximately degenerate. This degeneracy is lifted by radiative effects. The fermions receive mass corrections from the gauge interactions (with gauge bosons and adjoint scalars) and Yukawa interactions. All of these give positive mass shift.

The gauge fields and spinless adjoints receive mass corrections from the self-interactions and gauge interactions. Gauge interactions with fermions give a negative mass shift. While the self-interactions give positive mass shift with different strength with respect to the former. However, masses of the hypercharge gauge boson $B_\mu^{(j,k)}$ and the corresponding scalar $B_H^{(j,k)}$ receive only negative corrections from fermionic loops. Numerical computation shows that the lightest KK particle is the spinless adjoint $B_H^{(1,0)}$, associated with the hypercharge gauge boson. As a result, 2UED model gives rise to a scalar dark matter.

2.1 $(1,0)$-mode electroweak sector of 2UED

The $(1,0)$-mode electroweak sector of 2UED consists of $(1,0)$-mode gauge bosons ($B_\mu^{(1,0)}$, $W_\mu^{3(1,0)}$ and $W_\mu^{\pm(1,0)}$), spinless adjoints ($B_H^{(1,0)}$, $W_H^{3(1,0)}$ and $W_H^{\pm(1,0)}$) of $U(1)$ and $SU(2)$ gauge group respectively, $(1,0)$-mode KK excitations of the SM leptons and $(1,0)$-mode excitations of the Higgs doublet. In the previous section we have qualitatively discussed the effects of radiative corrections on the mass spectrum. After incorporating the radiative effects, approximate expressions for the masses at the $(1,0)$ level can be written as

$$\begin{aligned} M_{L_+} &\simeq 1.04\ R^{-1}, & M_{E_-} &\simeq R^{-1}, \\ M_{B_\mu} &\simeq 0.97\ R^{-1}, & M_{B_H} &\simeq 0.86\ R^{-1}, \\ M_{W_\mu} &\simeq 1.07\ R^{-1}, & M_{W_H} &\simeq 0.92 R^{-1}. \end{aligned} \tag{6}$$

The numerical factors in the above expressions are almost independent of R^{-1} for $(1,0)$-mode leptons, gauge boson and spinless adjoint corresponding to $U(1)$ gauge group. However, masses of $SU(2)$ gauge bosons and spinless adjoints do have mild dependencies on R^{-1}. Detailed expressions for the one-loop corrected masses of KK particles in 2UED can be found in Ref. [18].

Decays of $(1,0)$-mode particles of 2UED have been previously investigated in details in Ref. [13]. Conservation of KK-parity allows $(1,0)$-mode particles to decay only into a $(1,0)$-mode particle and one or more SM particles if kinematically allowed. It is clear from Eq. (6) that $B_H^{(1,0)}$ is the lightest KK particle (LKP) in this theory. It is important to notice that, unlike in the case of 1UED, the LKP is a scalar in this scenario. Since $B_H^{(1,0)}$ is a stable particle and weakly interacting, it passes through the detector without being detected. Decays of all the $(1,0)$-mode particles thus result into one or more SM particles plus missing energy/momentum signature.

R^{-1} in GeV	300	350	400	450	480	500
$B_\mu \to l l B_H$	0.610	0.618	0.624	0.630	0.633	0.635
$B_\mu \to \gamma B_H$	0.390	0.382	0.375	0.369	0.364	0.362

Table 1: Branching fractions of B_μ in $l\bar{l}B_H$ and γB_H channel for different values of R^{-1}

Let us begin with the $U(1)$ gauge boson B_μ[4]. B_μ dominantly decays to two SM charged leptons and B_H. This is a tree level 3-body decay. Apart from this 3-body decay, loop induced decay into a photon and B_H has comparable branching fraction [13]. B_μ decay to

[4]From now on we will only concentrate on $(1,0)$-mode, thus drop the $(1,0)$ superscript.

$f\bar{f}B_H$ is 3-body decay mediated by corresponding $(1,0)$ mode fermion. Decay amplitude is proportional to the hypercharge of the fermions in consideration. As a result, $B_\mu \to \nu\bar{\nu}B_H$ and $B_\mu \to q\bar{q}B_H$ are suppressed compared to $B_\mu \to l\bar{l}B_H$. This is even applicable for $B_\mu \to u_R\bar{u}_RB_H$ decay (hypercharge of u_R is 4/3). This is accounted by the fact that in case of $B_\mu \to u\bar{u}B_H$, decay amplitude is suppressed by heavier $U^{(1,0)}$ propagator (than $L^{(1,0)}$ propagator in case of $B_\mu \to l\bar{l}B_H$). In fact decay amplitude is inversely proportional to the mass difference of B_μ and the propagator mass. In Table 1, we have tabulated the branching fractions of B_μ in $l\bar{l}B_H$ (where l includes $e,\ \mu$ and τ) and γB_H channel for different values of R^{-1}. $SU(2)$ spinless adjoints ($W_H^\pm,\ W_H^3$) can decay only to the B_H and SM particles. W_H^3 decays to a pair of SM leptons and B_H with equal branching ratio to charged leptons and neutrinos. Branching fraction to quark antiquark pairs is again negligible due to hypercharge and heavy $(1,0)$ mode quark propagator. $W_H^\pm$ decay with almost 100% branching ratio to $l\bar{\nu}_lB_H$ (l includes all 3 SM lepton generations). Branching fractions of $SU(2)$ spinless adjoints are independent of R^{-1}.

Particle	Branching fractions in			
	$0l + \not{E}$	$1l + \not{E}$	$2l + \not{E}$	$3l + \not{E}$
W_μ^3	0.16	0	0.72	0
$W_\mu^\pm$	0	0.55	0	0.42

Table 2: Branching fractions of $(1,0)$-mode $SU(2)$ gauge bosons in *multi lepton + missing energy ($\not{E}$)* channel for $R^{-1} = 500$ GeV

Since the $(1,0)$-mode $SU(2)$ gauge bosons ($W_\mu^\pm,\ W_\mu^3$) are heavier than $(1,0)$-mode leptons (see Eq. 6), they decay dominantly into $(1,0)$-mode lepton doublets and corresponding SM leptons [13]. As for example, W_μ^3 can decay into one of the six ($l_iL_i^{(1,0)}$ and $\nu_i\nu_i^{(1,0)},\ i = e,\mu,\tau$) channels with equal probability. Similarly, $W_\mu^\pm$ decays into one of the six possible decay modes ($l_i\nu_i^{(1,0)}$ and $\nu_iL_i^{(1,0)},\ i = e,\mu,\tau$) with branching fraction of 1/6 into each decay modes. The $(1,0)$-mode leptons are heavier than B_μ, B_H and $SU(2)$ spinless adjoints. Therefore, $L^{(1,0)},\ \nu^{(1,0)}$ can decay into the corresponding SM lepton and B_μ (B_H) or $SU(2)$ spinless adjoints. Following this decay chain, one can see that $(1,0)$-mode $SU(2)$ gauge bosons dominantly decay to B_H and one or more SM leptons. We have presented the branching fractions of $(1,0)$-mode $SU(2)$ gauge bosons in multi lepton plus missing energy channels for $R^{-1} = 500$ GeV in Table 2. Branching ratios of $SU(2)$ gauge bosons are almost independent over R^{-1}. As for example, branching fraction of $W_\mu^3 \to 2l + \not{E}$ increases by 0.11% when R^{-1} is changed from 300 to 500 GeV.

One may tempted to think that the existing bound of Z'-mass (present in an extension of the SM with an extra $U(1)$ symmetry) might be applicable also to B_μ (W_μ^3). For example, Z' can be produced at resonance at the Tevatron and can decay to e^+e^- or $\mu^+\mu^-$ pairs [19]. The present bound on Z'-mass is around 900 GeV. However, B_μ (W_μ^3) can not be produced singly (due to KK-parity conservation) from $p\bar{p}$ collisions. At the same time B_μ (W_μ^3), once produced, decays to some SM particles (photon or leptons) and B_H. As a result, any decay of B_μ (W_μ^3) is always associated with large missing momentum/energy. Thus the direct/indirect search limits on Z' are not applicable to B_μ (W_μ^3).

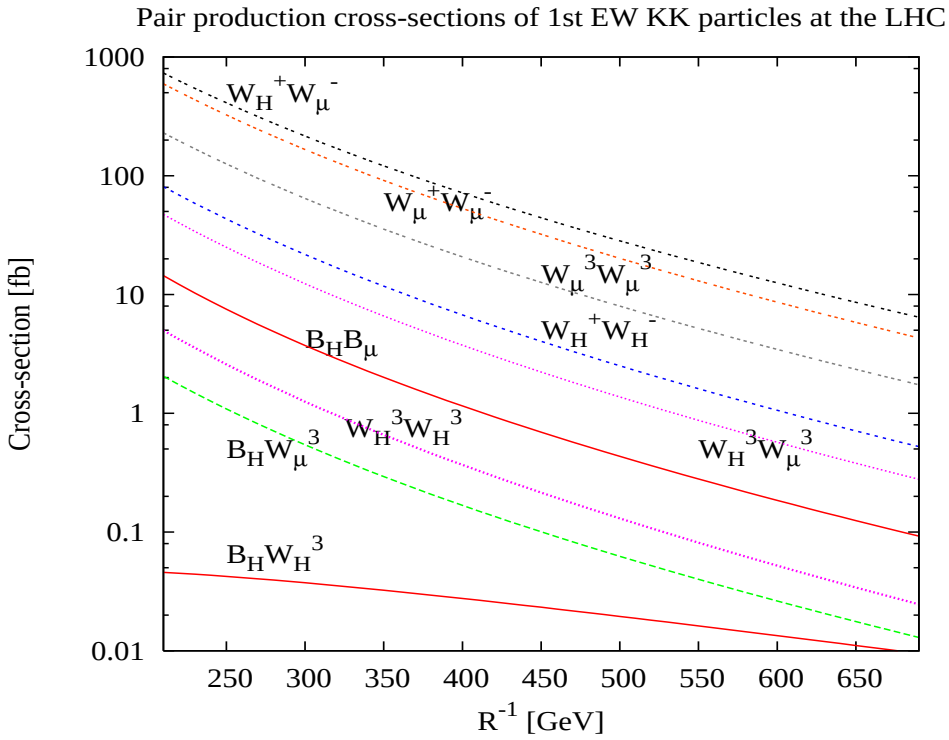

Figure 1: Pair production cross-sections of $(1,0)$-mode states at the LHC as a function of R^{-1}. CTEQ4L parton distribution functions are used to evaluate those cross-sections.

3 Signature of electroweak $(1,0)$-mode particles at the LHC

In this section, we will first discuss the production of electroweak $(1,0)$-mode particles of 2UED at the LHC. Phenomenology in 2UED is different and perhaps more complicated compared to 1UED due to the presence of spinless adjoints. In a previous work [15] we have studied the production (in the context of LHC) and decays of $(1,1)$-mode spinless adjoints in some details.

Due to the conservation of KK-parity, single production of $(1,0)$-mode particles is not possible. So they must be produced in pairs. All the $(1,0)$-mode electroweak gauge bosons and spinless adjoints have tree level couplings with an $(1,0)$-mode fermion and a SM fermion. These couplings arise from the compactification of 6D kinetic term for fermions, present in the 6D bulk Lagrangian. Two $(1,0)$-mode charged $SU(2)$ gauge bosons or spinless adjoints can couple to a SM photon or a SM Z-boson. Those couplings arise from the compactification of the kinetic term for 6D non Abelian gauge fields. All the vertices relevant for the pair production of $(1,0)$-mode electro-weak particles can be found in Appendix A. Pair production of $(1,0)$-mode electroweak gauge bosons or spinless adjoints at the LHC take place via the above mentioned interactions only. We have estimated the production cross-sections of the following pairs of neutral $(1,0)$-mode states: $\sigma(B_\mu, B_H)$, $\sigma(W^3_\mu, B_H)$, $\sigma(W^3_H, B_H)$, $\sigma(W^3_\mu, W^3_H)$, $\sigma(W^3_H, W^3_H)$, $\sigma(W^3_\mu, W^3_\mu)$; pairs of opposite charged $(1,0)$- modes: $\sigma(W^\pm_\mu, W^\mp_\mu)$, $\sigma(W^\pm_H, W^\mp_H)$, $\sigma(W^\pm_\mu, W^\mp_H)$ and pairs of one charged and one neutral states: $\sigma(W^\pm_\mu, W^3_\mu)$, $\sigma(W^\pm_\mu, W^3_H)$, $\sigma(W^\pm_H, W^3_\mu)$, $\sigma(W^\pm_H, W^3_H)$ in proton-proton collision at center-of-mass energy of

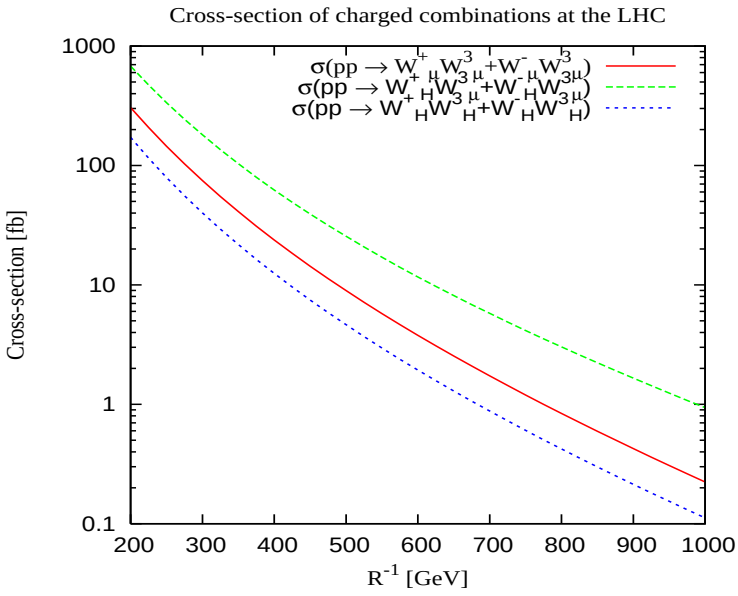

Figure 2: Production cross-sections for one charged + one neutral $(1,0)$-modes at the LHC as a function of R^{-1}. CTEQ4L parton distribution functions are used to evaluate those cross-sections.

14 TeV. CTEQ4L parton distribution functions [20] are used to numerically evaluate the above cross-sections. The factorization scale (for parton distribution functions) is fixed at the $(1,0)$-mode mass. For this study we have used one-loop corrected mass spectrum for $(1,0)$-mode particles given in Eq. (6).

The production cross-sections of two neutral $(1,0)$-mode or two oppositely charged $(1,0)$-mode final particles are presented in Fig. 1 as function of R^{-1}. The processes presented in Fig. 1, apart from being completely driven by electroweak couplings, are initiated by a quark and an antiquark. LHC, being a proton-proton collider, antiquarks can only arise from sea-excitations. Consequently, at the energy scale of our interest, the density of antiquarks inside a proton is small compared to quarks. This makes the above cross-sections small.

Production cross-sections of $U(1)$ spinless adjoint (B_H) in association with $SU(2)$ spinless adjoint (W_H^3) or gauge boson (W_μ^3) are smallest among the others. $B_H W_H^3$ (W_μ^3) pair production cross-section vary from 0.05 (2.5) fb to 0.01 fb as as we vary R^{-1} from 200 to 650 (700) GeV. $\sigma(W_H^3 W_H^3)$ and $\sigma(B_\mu B_H)$ are large compared to the previous two but the numerical values are not very promising. $W_H^3 W_H^3$ ($B_\mu B_\mu$) production cross-section varies from 8.75 (14.4) fb to 0.06 (0.09) fb as we vary R^{-1} from 200 to 690 GeV. At the parton level, $q\bar{q} \to B_H W_H^3$ (W_μ^3) or $W_H^3 W_H^3$ process is mediated by an excited $(1,0)$-mode quark in the t (u)-channel. Since $SU(2)$ gauge fields in 4D (6D) couple only with left-handed (6D +ve chirality) fermions, only the +ve chirality $(1,0)$-mode fermion $Q_+^{(1,0)}$ contributes in t (u)-channel. The coupling of a $(1,0)$-mode $U(1)$ gauge boson or spinless adjoint with an $(1,0)$-mode quark and a SM quark is proportional to the hypercharge of the corresponding quark. Due to small hypercharge of the quarks, processes involving one or two $U(1)$ gauge boson or spinless adjoint are suppressed at hadron collider.

Rest of the cross-sections, shown in Fig. 1, involves $SU(2)$ gauge bosons and spinless adjoints. These cross-sections are large even for larger value of R^{-1}. As for example,

cross-section for $W_\mu^\pm W_H^\mp$ ($W_\mu^\mp$) production and W_μ^3 pair production varies from few hundred femtobarn to few femtobarn as we vary R^{-1} from 200 to 700 GeV.

The production cross-sections of one charged and one neutral $(1,0)$-modes are presented in Fig. 2. $W_\mu^\pm W_H^3$ and $W_H^\pm W_\mu^3$ production cross-sections vary from few hundred femtobarn to 1 fb as we vary R^{-1} from 200 GeV to 1 TeV. In Fig. 2 we have not presented the production cross-sections of charged $SU(2)$ gauge bosons or spinless adjoints in association with a $U(1)$ gauge boson or spinless adjoint. Those production cross-sections are very much suppressed compared to the others due to the small hypercharge of quarks.

Final State	Parton level sub-processes $q\bar{q} \to AB$
$2-lepton\ +\ \not{p}_T$	$B_\mu B_H$, $W_\mu^3 B_H$, $W_H^3 B_H$, $W_\mu^3 W_H^3$, $W_H^3 W_H^3$, $W_\mu^3 W_\mu^3$, $W_\mu^\pm W_\mu^\mp$, $W_H^\pm W_H^\mp$, $W_\mu^\pm W_H^\mp$
$3-lepton\ +\ \not{p}_T$	$W_\mu^\pm W_\mu^3$, $W_\mu^\pm W_H^3$, $W_H^\pm, W_\mu^3$, $W_H^\pm, W_H^3$

Table 3: List of parton level sub-processes that contribute to the $2-lepton\ +\ \not{p}_T$ and $3-lepton\ +\ \not{p}_T$ signal at the LHC.

After a very short discussion about the pair production cross-sections of $(1,0)$-mode electroweak bosons and spinless-adjoints, we will now analyze the possible signals of this sector at the LHC. Electroweak $(1,0)$-mode particles of 2UED exclusively decay to multi lepton and B_H. Only exception is the $U(1)$ gauge boson B_μ, which can decay into a photon and B_H. Therefore, the pair production of B_μ and production of B_μ in association with B_H give rise to two photon and one photon + $\not{p}_T$ signal respectively. One or two photon + $\not{p}_T$ signals are unique for 2UED. However, due to small hypercharge of quarks, these production cross-sections are small at the LHC. Thus it is not possible to detect photon plus $\not{p}_T$ signal over the SM background. Since the hypercharges of electron and positron are large, the production cross-sections of B_μ in association with a B_H is expected to be large at an e^+e^- collider. Therefore, $B_\mu B_H$ pair production may gives rise to interesting signals of 2UED at e^+e^- collider. We will consider this possibility in Section 4 in details.

Since all other electroweak $(1,0)$-mode spinless adjoints or gauge bosons almost exclusively decay to SM leptons and B_H, we concentrate on *two SM leptons* + $\not{p}_T$ signal resulting from the production of two neutral or two oppositely charged $(1,0)$-mode particles and *three SM lepton* + $\not{p}_T$ signal arising from the production of one charged plus one neutral $(1,0)$-mode states. In Table 3, we have listed all the parton level sub-processes that contribute (after decay) to the *two (three) SM leptons* + $\not{p}_T$ signal. The decays of electroweak $(1,0)$-modes are discussed in section 2.1 (see Table 1 and Table 2).

3.1 2-lepton + $\not{p}_T$ signal

2-lepton + $\not{p}_T$ signal arises from the production of two (both neutral or charged) $(1,0)$ mode electroweak particles (presented in Fig. 1). Since the tau lepton detection efficiency is significantly different from both electron and muon, the signal is summed over electron and muon only ($l = e,\ \mu$).

Kinematic Variable	Minimum value	Maximum value
$\Delta R(l^+l^-)$	0.3	-
$p_T^{l^+,l^-}$	10 GeV	-
η_{l^+,l^-}	-2.5	2.5
$\not{p}_T$	25 GeV	-
$M(l^+l^-)$	10 GeV	-

Table 4: Acceptance cuts on the kinematical variables for *2-lepton* + $\not{p}_T$ signal.

We have used a parton level Monte-Carlo computer code to evaluate the $2l + \not{p}_T$ and $3l+\not{p}_T$ cross-sections. To parametrize detector acceptance and enhance signal to background ratio , we have imposed kinematic cuts, listed in Table 4. It is important to mention that production of $(1, 0)$-mode lepton pairs and their decay to a SM lepton + B_H also contributes to the signal. However, production of $(1, 0)$-mode lepton pairs at a hadron collider is purely a s-channel process and thus is very much suppressed.

With the acceptance cuts, defined in Table 4, the total signal cross-section is small for the higher values of R^{-1}. As for example, the total signal cross-section is 19.46 fb for $R^{-1} = 450$ GeV. However, the difficulty in detecting the signals is not the small rate of production, but due to the large SM background which we will discuss in the following.

In the SM, the dominant contribution to $2l+\not{p}_T$ comes from the W-boson pair production, Z-boson pair production and production of a Z-boson in association with a virtual photon. $2l + \not{p}_T$ background can also come from the production of a WZ-pairs followed by leptonic decay of both W and Z where one of the charged lepton falls outside the detector coverage. However, with the acceptance cuts (listed in Table 4) this cross-section is estimated to be very small.

Kinematic Variable	Minimum value	Maximum value
$M(l^+l^-)$	10 GeV	85 GeV
$\Delta\Phi_{l^+l^-}$	-	177^0

Table 5: Selection cuts on the kinematical variables for *2-lepton* + $\not{p}_T$ signal.

It is important to notice that the signal, we are considering, consists of only two observable charged leptons which may come from ordinary Drell-Yan process. However, Drell-Yan production of lepton pairs is not accompanied by missing energy. So this kind of background can be removed simply by demanding a minimum value of the missing transverse momentum. Drell-Yan production of τ-lepton pairs and subsequent leptonic decays of τ provides a real background to 2UED signal. However, the leptons ($l = e,\ \mu$) resulting from the Drell-Yan production of τ pairs are almost back to back in the transverse plane. Therefore, this contribution can be completely removed by demanding an upper bound on the angle between leptons in the transverse plane.

The production $t\bar{t}$ pairs and subsequent semi-leptonic decays of both the top quarks also contributes to the $2l + \not{p}_T$ background where both the partons are either too soft to be identified as jets or fall outside detector coverage. We made an estimate of this background

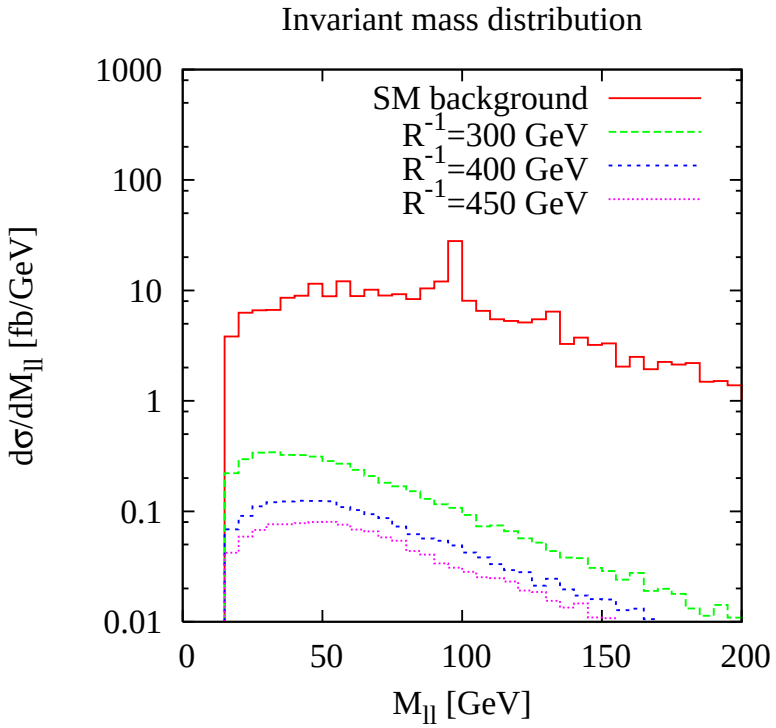

Figure 3: Invariant mass (of lepton pair) distribution of signal (for three different values of R^{-1}) and background (for *2-lepton plus* $\not{p}_T$ signal).

by demanding the partons can be identified as jets only if their $p_T > 30$ GeV[5].

The background from Z-boson pair production can be eliminated by rejecting events in which the invariant mass of the lepton pairs is close to the mass of Z-boson. Fig. 3 shows the invariant mass distribution for the SM background and signal. Z-pole is clearly visible in the SM background distribution. To extract signal from the SM background we impose the selection cuts listed in Table 5. The choice of selection cut on the invariant mass of the lepton pairs is largely aimed to reduce the contribution from the Z-boson pair production. With those selection cuts, listed in Table 5, the background, arises from production of $t\bar{t}$ pairs, is also found to be small. In Table 6, we have presented the background cross-sections after acceptance cuts (second column) and selection cuts (third column).

The dominant background to the $2l + \not{p}_T$ signal is W-boson pair production from quark-antiquark annihilation followed by leptonic decay of each of the W-bosons. It is difficult to choose a selection criteria which can completely remove this background without affecting the signal.

Signal cross-section for different values of R^{-1} are presented in Table 7 after applying the acceptance cuts (2nd column) and selection cuts (3rd column) respectively. The corresponding background cross-sections are also presented in Table 6. In order to quantify the ability of extracting signal event, $N_S = \sigma_S \mathcal{L}$, for a given integrated luminosity $\mathcal{L}$ over the SM background events, $N_B = \sigma_B \mathcal{L}$, we define the significance $S = N_S/\sqrt{N_B}$. It is clear

[5]We keep in mind that in LHC environment purely leptonic signal like ours are always come with soft jets. In our parton level analysis, we assume that unless the b-parton coming from t-decay have $p_T > 30$ GeV, it can not be identified as jets.

Contributing SM process	Cross-section in fb	
	After acceptance cuts	After selection cuts
$pp \to \tau\bar{\tau}$	216	4.7
$pp \to W^{\pm}Z$	2.1	0.4
$pp \to t\bar{t}$	22.5	8.13
$pp \to W^+W^- + \gamma^*Z$	1220	444

Table 6: Standard model background cross-sections for *2-lepton* + $\not{p}_T$ signal.

R^{-1} in GeV	Signal cross-section in fb	
	After acceptance cut	After selection cut
300	24.4	18.5
350	19.1	11.4
400	10	7.3
450	6.7	4.7

Table 7: *2-lepton* + $\not{p}_T$ signal cross-sections for different values of R^{-1}.

from the numbers in Table 7 that, with 100 fb^{-1} luminosity, more than 5σ discovery of the signal is possible upto $R^{-1} = 350$ GeV.

3.2 3-lepton + $\not{p}_T$ signal

In the frame work of 2UED, *3-lepton* + $\not{p}_T$ signal results from the production of a neutral $(1,0)$-mode gauge boson or spinless adjoint in association with a charged $(1,0)$-mode $SU(2)$ gauge boson or spinless adjoint (presented in Fig. 2). As for example, the production of a neutral gauge boson or spinless adjoint in association with a charged $SU(2)$ spinless adjoint and the subsequent decay of the charged adjoint in *1-lepton* + $\not{p}_T$ channel and neutral particle in *2-lepton* + $\not{p}_T$ channel give rise to *3-lepton* + $\not{p}_T$ signal, $pp \to W_H^{\pm}W_{\mu}^3$ $(W_H^3) \to (l^{\pm}B_H)(l^+l^-B_H)$. However, the decay of $(1,0)$-mode $SU(2)$ charged gauge bosons into *1-lepton* + $\not{p}_T$ channel and *3-lepton* + $\not{p}_T$ channel are equally probable as can be seen from Table 2. Therefore, for $W_{\mu}^{\pm}W_{\mu}^3$ (W_H^3) production, both the invisible decay and *2-lepton* + B_H decay of W_{μ}^3 (W_H^3) contributes to the signal. Instead of including all three SM lepton generations, in this part of the work we consider only first two generations of SM leptons $(l = e,\ \mu)$. We impose following selection criteria, listed in Table 8, on the kinematical variables after ordering the leptons according to their p_T hardness $(p_T^{l_1} \leq p_T^{l_2} \leq p_T^{l_3})$.

In the SM, the dominant contribution to *3-lepton* + $\not{p}_T$ comes from the production of W-boson in association with a Z-boson or a virtual photon. The WZ production is characterized by a peak in the invariant mass distribution of the lepton pairs at the Z-boson mass. Fig. 4 shows the invariant mass (of three possible combinations of leptons) distributions for signal (for $R^{-1} = 500$ GeV) and background. Therefore, the contributions from WZ production can be eliminated by rejecting the events in which the invariant mass of any lepton pair is close to the mass of the Z-boson. However, it is difficult to introduce an event selection criteria to eliminate the $W\gamma^*$ contribution without affecting the signal. However, the lepton pairs coming from γ^* are in general soft an try to be collinear to each other. Hence a cut on

Kinematic Variable	Minimum value	Maximum value
$\Delta R(l_i l_j),\ i \neq j$	0.3	-
$p_T^{l_i}$	10 GeV	-
η_{l_i}	-2.5	2.5
$\not{p}_T$	25 GeV	-

Table 8: Acceptance cuts on the kinematical variables for *3-lepton* + $\not{p}_T$ signal with $i, j = 1, 2, 3$ and $l = e,\ \mu$.

Applied Cuts	Background cross-section in fb	Signal cross-section in fb			
		R^{-1} in GeV			
		400	500	550	600
Acceptance cuts	145	8.83	4.51	3.29	2.44
$10\ GeV < p_T^{l_1} < 50\ GeV$, $15\ GeV < p_T^{l_2} < 50\ GeV$, $p_T^{l_3} > 20\ GeV$	99.7	7.2	3.71	2.74	1.98
$20\ GeV < M_{l_1 l_2} < 70\ GeV$, $\lvert M_{l_1 l_3} - m_Z \rvert > 10\ GeV$, $\lvert M_{l_2 l_3} - m_Z \rvert > 10\ GeV$	6.39	4.8	2.46	1.72	1.23

Table 9: *3-lepton* + $\not{p}_T$ signal (for different values of R^{-1}) and corresponding SM background after three sets of successive cuts. m_Z is the mass of Z-boson.

the invariant mass of the $l_1 l_2$ can remove a large part of this background.

To extract the signal from the SM background we have introduced a set of cuts, listed in Table 9. It is important to notice that the signal leptons results from the decay of a heavy particle (such as $W_\mu^\pm$, $W_H^\pm$, W_μ^3 and W_H^3) into another heavy particle (B_H) plus one or more SM leptons. Therefore, the SM leptons most of the time carry small amount of energy. However, the background leptons arises from the decay of W and Z or a virtual photon. Consequently, the leptons from the decay of W or Z bosons are not very much soft. We have exploited this feature of the signal to enhance the signal to background ratio. In Table 9, we have imposed some upper bounds on the transverse momentum and invariant mass of leptons. We have also excluded the some region of the invariant mass distribution near Z-boson mass to suppress the reducible background arises from WZ production. Table 9 also include signal (for different values of R^{-1}) and SM background cross-sections after the selection cuts (p_T cuts and cuts on the invariant mass of the three lepton pairs). Here it is important to mention that the transverse mass distributions of the three background leptons also show a characteristics W-boson peak. However, we found that the cuts on the invariant masses are more effective than the cuts on the transverse masses. Numbers presented in Table 9 clearly indicates that, at 100 fb^{-1} luminosity of the LHC, 5σ discovery of the *3-lepton* + $\not{p}_T$ signal is possible upto $R^{-1} = 600$ GeV.

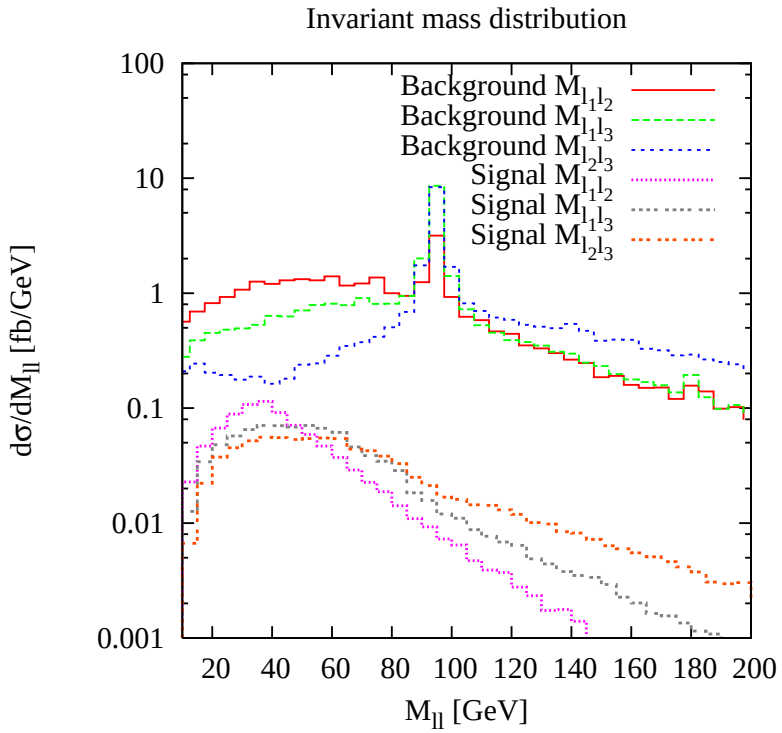

Figure 4: Invariant mass distribution of signal (for $R^{-1} = 500$ GeV) and background (for *3-lepton* + $\not{p}_T$ signal).

4 Signature of $(1,0)$-mode $U(1)$ sector at the ILC

The importance of B_μ production in association with a B_H has been briefly mentioned in the section 3. Since the couplings of $U(1)$ gauge boson or spinless adjoint with quarks are suppressed by the hypercharge of the respective quark, the $B_\mu B_H$ pair production cross-section is very small at LHC. Therefore, if not possible to study the signals from $B_\mu B_H$ pair production at the LHC. However, the couplings of $U(1)$ gauge boson or spinless adjoint with leptons are enhanced by the hypercharges of the corresponding leptons. One can expect a higher rate of production for $U(1)$ gauge boson and spinless adjoint at a e^+e^- collider. In this section we will discuss the prospect of $B_\mu B_H$ pair production at a future linear e^+e^- collider.

Both B_μ and B_H can couple to a $(1,0)$-mode lepton and a SM lepton. The couplings arise from the compactification of 6D kinetic term for 6D leptons and can be found in Appendix A. At an e^+e^- collider, they can be directly produced in pairs,

$$e^+ + e^- \;\rightarrow\; B_\mu + B_H, \tag{7}$$

which proceeds via the exchange of an $(1,0)$-mode electron ($E_+^{(1,0)}$ or $E_-^{(1,0)}$) in t (u) channel. The numerical values of the cross-sections are presented in Fig. 5 as a function of R^{-1} for two different values of e^+e^- center-of-mass energies.

B_μ dominantly decays to two SM leptons and a LKP resulting into 2-leptons and missing energy signal. However, this is not the only source of 2-lepton and missing energy in 2UED. Pair productions of almost all combinations of electroweak gauge bosons and spinless adjoints

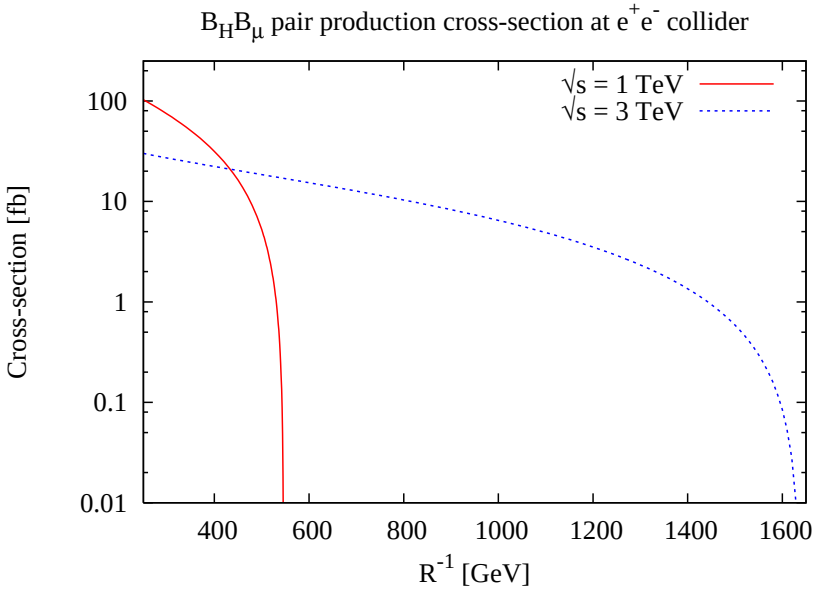

Figure 5: $B_\mu B_H$ pair production cross section as a function of the compactification radius R^{-1} for 1 TeV (solid line) and 3 TeV (dashed line) center-of-mass energy of e^+e^- collider.

give rise to 2-lepton and missing energy final state. In fact, the largest contribution to 2-lepton and missing energy, in 2UED, comes from the pair production of $(1,0)$-mode electrons and their subsequent decays to SM electrons and LKP [16]. However, in this work we will concentrate on the other decay mode of B_μ, i.e to a photon and LKP. We are interested in analysing the $\gamma + \not{E}$ signal.

Single photon + missing energy signal is particularly interesting because this signal is the characteristics of this theory. Since the structure of 2UED theory and 1UED theory are almost identical, they give rise to similar kind of signals at colliders. However, *single photon + missing energy* signal is one of the very few spectacular signals which can distinguish 1UED and 2UED. In 1UED similar kind of signal can only arise from the production of LKP in association with a photon. In fact, all those theories which include a dark matter candidate can give rise to *single photon + missing transverse momentum* signal[6] via the radiative production of the dark matter candidate. As for example, radiative production of lightest supersymmetric particles (LSP) in different R-parity conserving supersymmetric models gives rise to single photon plus missing transverse momentum signal. However, all those radiative production processes are suppressed by the square of an additional electron photon coupling. Moreover, photons from radiative productions are predominantly soft or collinear. Therefore, the detector acceptance cuts on photon energy and rapidity almost remove the contributions from radiative pair production of LKP or LSP.

Radiative neutrino production ($e^+e^- \to \nu_l\bar{\nu}_l\gamma$) is the major SM background to the signal. Some acceptance cuts on the signal and background are listed in Table 10. It is worthwhile to mention that photon rapidity cut reduces another potentially dangerous background namely the radiative Bhabha scattering, $e^+e^- \to e^+e^-\gamma$, where both the final state leptons escape

[6]It is important to mention that in MSSM the production of lightest nutralino ($\tilde{\chi}_1$) in association with the next to lightest nutralino ($\tilde{\chi}_2$) and subsequent radiative decay of $\tilde{\chi}_2$ to a photon and $\tilde{\chi}_1$ [21] gives rise to the similar kind of signal. It is beyond the scope of this article to compare this process with 2UED.

along the beam pipe.

Kinematic Variable	Minimum value	Maximum value
η_γ	-2.5	2.5
E_γ	10 GeV	-

Table 10: Acceptance cuts on the photon rapidity η_γ and photon energy E_γ

We have estimated background cross-sections for two center-of-mass energies of e^+e^- collider. In Table 11, we have presented the numerical values of the signal and background cross-sections for three different values of R^{-1} at 1 TeV and 3 TeV e^+e^- collider. Table 11 shows that the signal cross-sections (at 1 TeV) are small in comparison with the background for the values of R^{-1} close to the kinematic limit of the collider. The situation is even worse for 3 TeV collider. Here the signal is much smaller compared to the background even for the smaller value of R^{-1}.

$\sqrt{s}$ = 1 TeV			$\sqrt{s}$ = 3 TeV		
R^{-1} in GeV	Signal in fb	Background in fb	R^{-1} in GeV	Signal in fb	Background in fb
300	26.03		500	6.21	
400	11.15	3609	1000	2.28	4248
500	1.87		1500	0.21	

Table 11: Signal and background cross-section at 1 TeV and 3 TeV collider after imposing acceptance cuts on the photon rapidity and energy.

Pair production of B_H in association with a photon also gives rise to *single photon + missing energy* signal.

$$e^+ + e^- \ \rightarrow \ \gamma + B_H + B_H \tag{8}$$

However, cross-section of this process is suppressed w.r.t. the former. Also the photons, radiated from incident electron or positron, are predominantly soft or collinear. So the cuts on photon rapidity and energy completely remove this contribution. We have estimated $\gamma B_H B_H$ contribution at $R^{-1} = 500$ GeV and it is found that this is suppressed by a large factor (~ 200 at an 1 TeV collider) compared to the $B_\mu B_H$ contribution.

4.1 Beam polarization dependence of signal and background

One of the merits for an e^+e^- collider is the possibility of highly polarized e^+ and e^- beams. Here it is important to mention that the maximum 80% longitudinal beam polarization of electron beam and 60% longitudinal beam polarization of positron beam is possible at the ILC and CILC [22]. Denoting the average $e^\pm$ beam polarization by $P_\pm$, the polarized squared matrix element can be constructed [22] based on the helicity amplitude $\mathcal{M}_{\sigma_{e^+}\sigma_{e^-}}$:

$$\begin{aligned}\overline{\sum|\mathcal{M}|^2} &= \frac{1}{4}[(1-P_-)(1-P_+)|\mathcal{M}_{LL}|^2 + (1-P_-)(1+P_+)|\mathcal{M}_{LR}|^2 \\ &+ (1+P_-)(1-P_+)|\mathcal{M}_{RL}|^2 + (1+P_-)(1+P_+)|\mathcal{M}_{RR}|^2]\end{aligned} \tag{9}$$

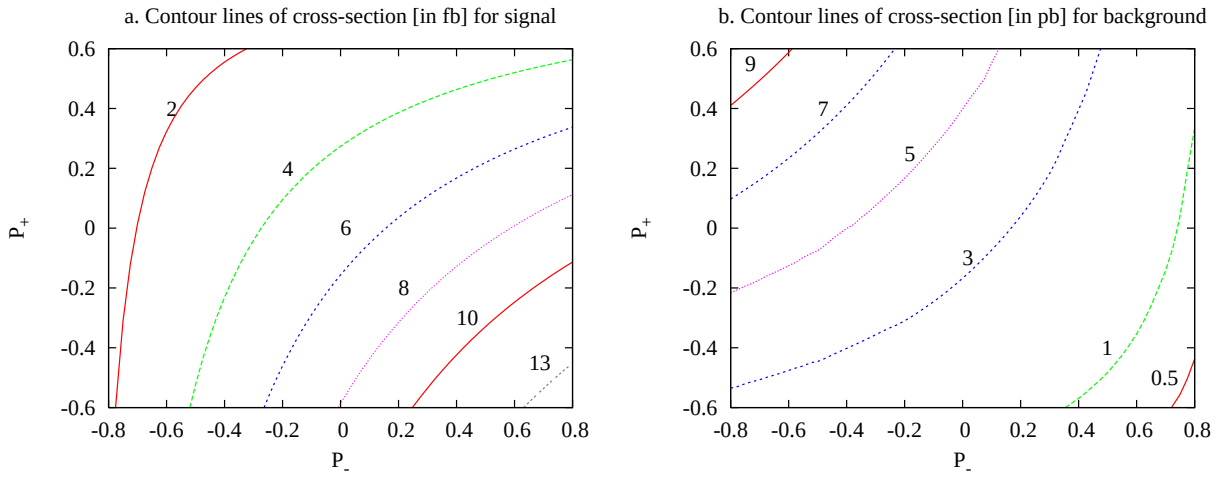

Figure 6: The beam polarization dependence of (a) $\sigma(e^+e^- \to B_\mu B_H)$ for $R^{-1} = 500$ GeV and (b) SM background at 1 TeV center-of-mass energy of e^+e^- collider.

Eq. (9) clearly indicates that $P_\pm = 1$ corresponds to purely right handed and $P_\pm = -1$ corresponds to purely left handed electron or positron beam. Since the electroweak interactions of both SM and 2UED are chiral, it may be possible to suppress SM background compared to the 2UED signal by proper choice of beam polarization.

Since electron is nearly massless, the background amplitude vanishes unless electron and positron have opposite helicity ($\mathcal{M}^B_{LL} = \mathcal{M}^B_{RR} = 0$). Production of B_μ in association with a B_H is mediated by a massive $(1,0)$-mode electron ($E^{(1,0)}_\pm$) exchanged in t (u)-channel. However, the structure of 2UED is such that $E^{(1,0)}_+$ ($E^{(1,0)}_-$) can only couple to a left (right) handed electron or a right (left) handed positron and a $(1,0)$-mode gauge boson or spinless adjoint. Therefore, here also the amplitude vanishes for the same helicity of electron and positron beam. Since the hypercharge of right handed leptons are larger than left handed leptons by a factor of 2, the coupling of a right (left) handed electron (positron) with $E^{(1.0)}_-$ and $B^{(1,0)}_H$ or $B^{(1,0)}_\mu$ is enhanced by a factor two than the coupling of a left (right) handed electron (positron) with $E^{(1.0)}_+$ and $B^{(1,0)}_H$ or $B^{(1,0)}_\mu$. Thus the contribution from $E^{(1,0)}_-$ exchange to the cross-section is about a factor 16 larger than the $E^{(1,0)}_+$ contribution. The background process mainly proceeds via W boson exchange. Thus positive electron beam polarization, P_-, and negative positron beam polarization, P_+, enhance signal cross-section and reduce background at the same time. We have presented the beam polarization dependence of the cross-section $\sigma(e^+e^- \to B^{(1,0)}_\mu B^{(1,0)}_H)$ for $R^{-1} = 500$ GeV and $\sqrt{s} = 1$ TeV in Fig. 6a. Fig. 6b shows the polarization dependence of background cross-section $\sigma(e^+e^- \to \gamma\nu_l\bar{\nu}_l)$ at 1 TeV center-of-mass energy of e^+e^- collider.

We have used the same definition of the statistical significance as defined in the Section 3.1. Fig. 7 shows the polarization dependence of the significance for $\gamma + \not{E}_T$ signal at $R^{-1} = 500$ GeV, $\mathcal{L} = 500\ fb^{-1}$ and $\sqrt{s_{ee}} = 1$ TeV. In going from unpolarized beam $(P_-, P_+) = (0, 0)$ to partially polarized beam $(P_-, P_+) = (0.8, -0.6)$, the significance is enhanced by a factor $\sim$ 8 to $S = 6$. But the situation is not that hopeful for 3 TeV collider. At $R^{-1} = 1.5$ TeV the significance enhanced by a factor ~ 10 to $S = 0.7$ as we vary beam polarization from $(P_-, P_+) = (0, 0)$ to $(P_-, P_+) = (0.8, -0.6)$.

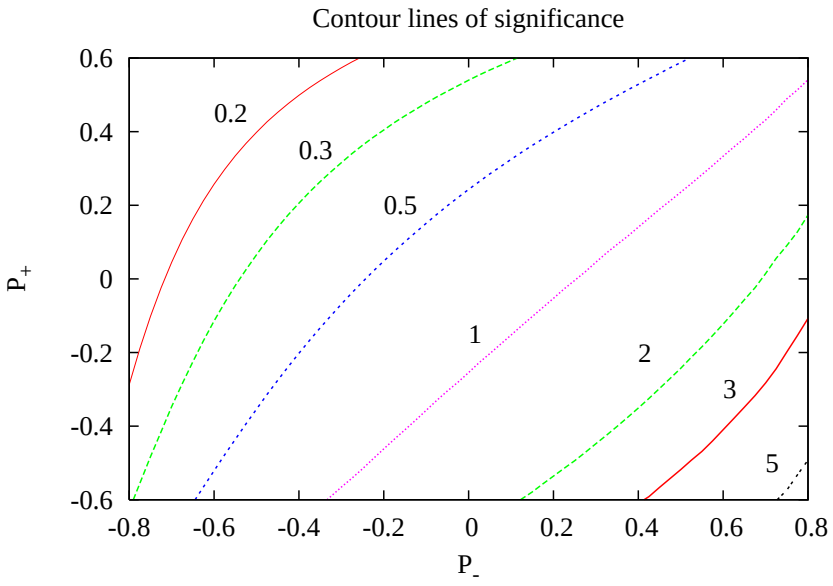

Figure 7: Contour lines of the significance for $e^+e^- \to B_\mu B_H$ at $R^{-1} = 500$ GeV, $\sqrt{s} = 1$ TeV and $\mathcal{L} = 500\ fb^{-1}$.

After exploiting the beam polarization to enhance the signal, further suppression of background can be possible by looking at some kinematic distributions. In Fig. 8a we have presented the photon rapidity (η_γ) distribution for signal and background for $\sqrt{s_{ee}} = 1$ TeV. Fig. 8a shows that signal events are dominantly in the central rapidity region. Therefore, the cut on photon rapidity (in Table 10) suppress the SM background compared to the signal.

Since W-boson can only couple with left (right) handed electrons (positrons), the selection of beam polarization, $P_- = 0.8$, $P_+ = -0.6$, reduces the background via t-channel W-boson exchange. Due to the hypercharge, coupling of Z-boson with right (left) handed electrons (positrons) is larger than left (right) handed electrons (positrons). So the background from radiative production of Z-boson increases as we select positive electron beam polarization and negative positron beam polarization. However, radiative production of Z-boson is characterized by a peak in photon energy distribution at $E_\gamma = \frac{s-m_Z^2}{2\sqrt{s}}$. Fig. 8b shows E_γ distribution of signal and background at an 1 TeV center-of-mass energy of e^+e^- collider for the previous choice of P_- and P_+ and an integrated luminosity of $\mathcal{L} = 500\ fb^{-1}$.

We will first concentrate on the E_γ distribution of the signal. The decay $B_\mu \to \gamma B_H$ gives rise to a monoenergetic photon with energy $E_\gamma^0 = \frac{m_{B_\mu}^2 - m_{B_H}^2}{2m_{B_\mu}}$ at the rest frame of B_μ. Photon energy spreads out due to the velocity of the produced B_μ, resulting into a box shaped distribution. In a fixed center-of-mass energy e^+e^- collider, as we increase R^{-1}, $B_\mu B_H$ pair production approaches towards the kinematical threshold of the collider. Therefore, increasing R^{-1} implies decreasing velocity of B_μ and decreasing width of box shaped E_γ distribution.

In Table 12, the total number of signal events are presented for different values of R^{-1} and for two center-of-mass energies of e^+e^- collider. In Table 12, we have used the following event selection criteria. In a particular bin and also in one of its adjacent bins, if the number of events are greater than the SM background events plus 1σ fluctuation of SM background

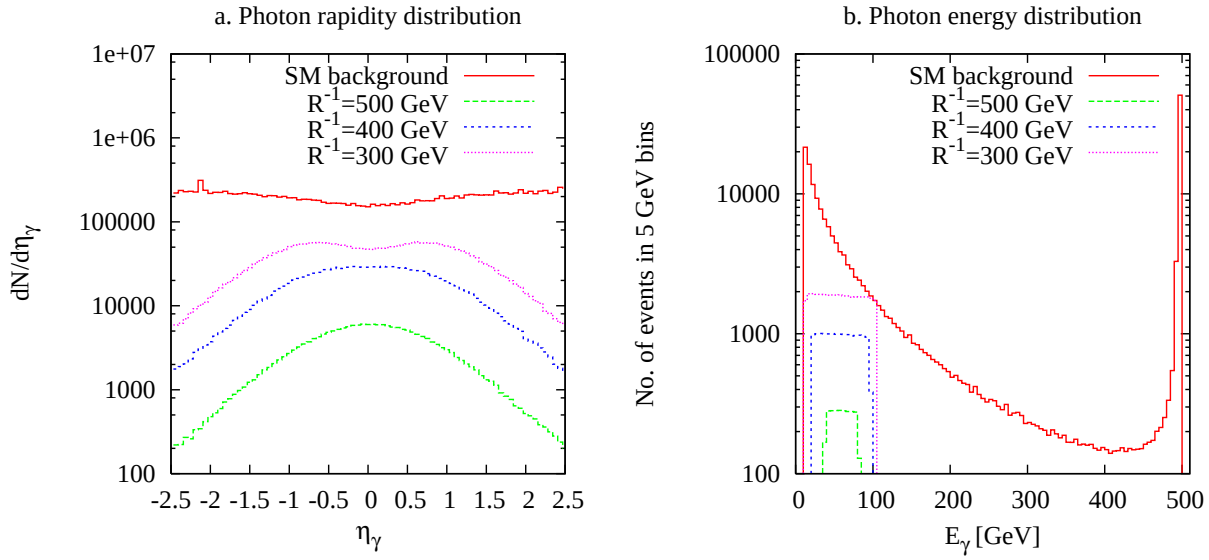

Figure 8: Photon (a) rapidity distribution and (b) energy distribution for $\gamma + \not{E}$ events for signal (dotted, dashed, long dashed histogram) and background (solid histogram) at $\sqrt{s} = 1$ TeV, $\mathcal{L} = 500\ fb^{-1}$ and beam polarization $(P_-, P_+) = (0.8, -0.6)$.

events, we take the background subtracted events in that particular bin as the signal events. The total number of signal events are the sum of signal events in the above mentioned bins. The sum of the background events in those bins are also presented in Table 12 with their 1σ fluctuation.

Now we will discuss one more interesting feature of this signal. For a fixed center-of-mass energy e^+e^- collider, the width (ΔE_γ) of photon energy distribution is directly related to the R^{-1} by the relation

$$0.0405\ R^{-4} - 3.361\ s\ R^{-2} + s^2\ =\ 87.3439\ s\ (\Delta E_\gamma)^2 \tag{10}$$

From the measurement of the width of photon energy distribution experimentally, one can calculate R^{-1} by solving Eq. (10). But, experimentally the measurement of width will be challenging task. Particularly, the measurement of the lower kinematical end point $(E_{\gamma,min})$ of photon energy distribution will be difficult due to the huge SM background in the lower E_γ region and detector limitation of measuring very low energy photon. However, the upper kinematical end point, $E_{\gamma,max}$, of photon energy distribution can be relatively easily measured. $E_{\gamma,max}$ is related with R^{-1} by the following relation

$$\begin{aligned} &0.107\left(0.0405\ R^{-4} - 3.361\ s\ R^{-2} + s^2\right)^{\frac{1}{2}} + \\ &0.0535\left(0.0405\ R^{-4} + 0.4026\ s\ R^{-2} + s^2\right)^{\frac{1}{2}} = \sqrt{s}\ E_{\gamma,max} \end{aligned} \tag{11}$$

With the measured value of $E_{\gamma,max}$, Eq. (11) can again be solved numerically to estimate the value of R^{-1}.

$\sqrt{s_{ee}}$ = 1 TeV			$\sqrt{s_{ee}}$ = 3 TeV		
R^{-1} in GeV	Signal Events	Background Events	R^{-1} in GeV	Signal Events	Background Events
300	35291	114760 (339)	500	8279	141378 (376)
350	24192	93193 (305)	800	4528	69964 (264)
400	15141	75194 (274)	1000	2835	53056 (230)
450	7851	61669 (248)	1200	1154	21485 (146)
500	2538	40369 (201)	1250	755	12735 (113)
520	999	25538 (160)	1300	484	8182 (90)

Table 12: Number of $\gamma + \not{E}$ signal and SM background events for two values of e^+e^- center-of-mass energy assuming 500 fb^{-1} integrated luminosity. 1σ fluctuations of the background events are also shown in the brackets.

5 Conclusion

To summarise, we have investigated possible signatures of $(1,0)$-mode electroweak particles in the framework of 2UED model in the context of LHC and also at a future e^+e^- collider. KK-parity allows only the pair production of these particles. Once they are produced in pairs, they give rise to *multi lepton + missing transverse momentum* signal. The only exception is $B_\mu B_H$ production which gives rise *single photon + missing transverse momentum* signal.

At the LHC we study *two* and *three (charged SM) lepton + missing transverse momentum* signal. We have estimated contributions to the signal from different combinations of $(1,0)$-mode gauge bosons and spinless adjoints pair production at the LHC. We have also estimated the SM background contributions to *two* and *three charged lepton + missing transverse momentum* signal. We find that with 100 fb^{-1} luminosity of the LHC, *two (three) lepton + missing transverse momentum* signal from the $(1,0)$-mode electroweak sector of 2UED is greater than 5σ standard deviation of the SM background upto $R^{-1} = 400$ (600) GeV.

At e^+e^- collider we only concentrate on $B_\mu B_H$ production. $B_\mu B_H$ production cross-section is large due to the large hypercharge of electron and positron. We have only investigated *single photon + missing energy* signal at a future e^+e^- collider. The SM model contribution ($e^+e^- \to \gamma\nu\bar{\nu}$) to the *single photon + missing energy* is huge. Kinematical cuts (cuts on photon energy) can remove only those part of background which arises from the radiative production of Z-boson. The dominant contribution to $e^+e^- \to \gamma\nu\bar{\nu}$ arises from t-channel W-boson exchange. Fortunately, the choice of positive electron beam polarization and negative positron beam polarization reduces t-channel W-boson exchange contribution to the background and at the same time enhance the signal cross-section. In our analysis, we choose 80% positive electron beam polarization and 60% negative positron beam polarization ($(P_-, P_+) = (0.8, -0.6)$). We find that for 500 fb^{-1} luminosity of e^+e^- collider, *single photon + missing energy* signal form $e^+e^- \to B_\mu B_H$ production and $B_\mu \to \gamma B_H$ decay is greater than 5σ standard deviation of the SM background, almost upto the kinematic limit of the collider. Since the photon arises from the B_μ decay, the kinematical endpoints of photon energy distribution only depend on the center-of-mass energy, $\sqrt{s_{ee}}$, of e^+e^- collider and R^{-1}. So from the experimental measurement of one of the kinematical end points (preferably upper kinematical end point) of photon energy distribution, one can estimate R^{-1}. We find very high sensitivity of R^{-1} with the upper kinematical end point of photon

energy distribution. Therefore, precise determination of photon energy at electromagnetic calorimeter will enhance the accuracy R^{-1} estimation.

Acknowledgments KG acknowledges the support from Council of Scientific and Industrial Research, Govt. of India (Sanction No. 09/028(0675)/2006 EMR-1).

Appendix A : Relevant Feynman Rules

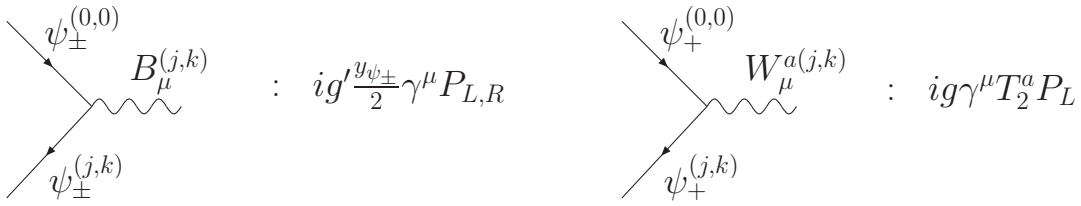

Figure 9: Feynman rules of KK-number conserving interactions of a (j,k)-mode gauge boson ($B_\mu^{(j,k)}$ and $W_\mu^{3,\pm(j,k)}$) with the (j,k)-mode fermion and the corresponding SM fermion. g and g' are the $SU(2)$ and $U(1)$ gauge coupling constant respectively and T_2^a's are the generators of the $SU(2)$ gauge group. $y_{\psi_\pm}$ is the hypercharge of the fermion $\psi_\pm$.

In this section we show the Feynman rules that are relevant for the production of the $(1,0)$-mode electroweak particles at the hadron collider and electron-positron collider. To make this discussion more general, we present electroweak vertices involving two (j,k)-mode particles and a SM particle. Corresponding vertices involving $(1,0)$-mode can be easily inferred from the Feynman rules given in Figs. 9, 10, 11.

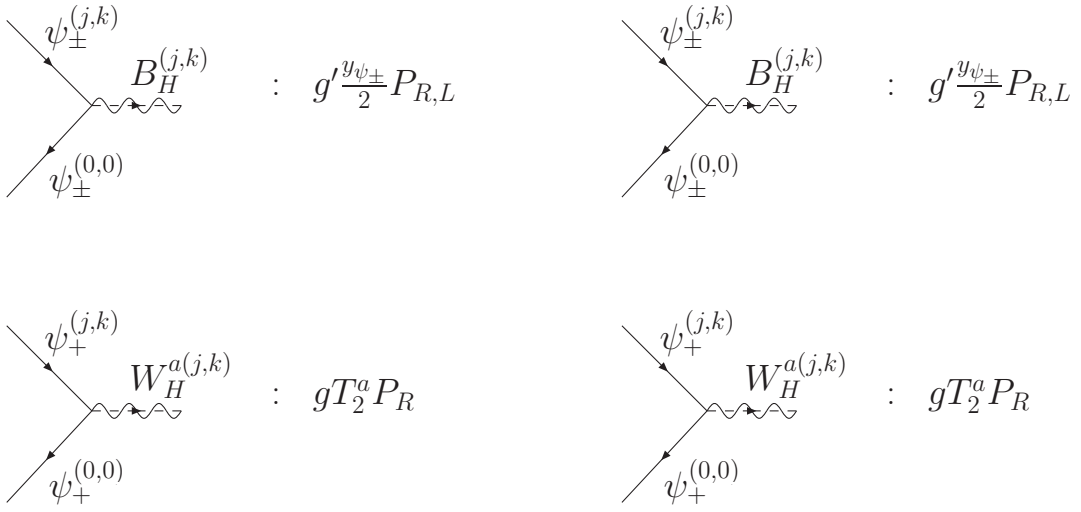

Figure 10: Feynman rules of KK-number conserving interactions of a (j,k)-mode spinless adjoint ($B_H^{(j,k)}$ and $W_H^{3,\pm(j,k)}$) with the (j,k)-mode fermion and the corresponding SM fermion.

Compactification of the 6-dimensional kinetic terms for fermions and integration over the compactified co-ordinates results KK-number conserving interactions involving a KK gauge boson (spinless adjoint) and two fermions. In Fig. 9, we have presented $V_\mu^{(j,k)}\psi^{(j,k)}\bar{\psi}^{(0,0)}$ ($V_\mu^{(j,k)}$ corresponds to $B_\mu^{(j,k)}$ or $W_\mu^{3,\pm(j,k)}$) vertices and Fig. 10 shows $V_H^{(j,k)}\psi^{(j,k)}\bar{\psi}^{(0,0)}$ ($V_H^{(j,k)}$ corresponds to $B_H^{(j,k)}$ or $W_H^{3,\pm(j,k)}$) vertices. In Fig. 9 and Fig. 10, + and − label the 6-dimensional chiralities of the fermion as discussed in section 2 (see Eq. 5).

3-point interaction involving only one SM vector boson (γ, Z or $W_\mu^\pm$) and two (j,k)-mode $SU(2)$ spinless adjoints ($W_H^{3,\pm(j,k)}$) arises from the compactification of the self-interacting part of the 6-dimensional $SU(2)$ gauge fields. Corresponding vertices are presented in Fig. 11.

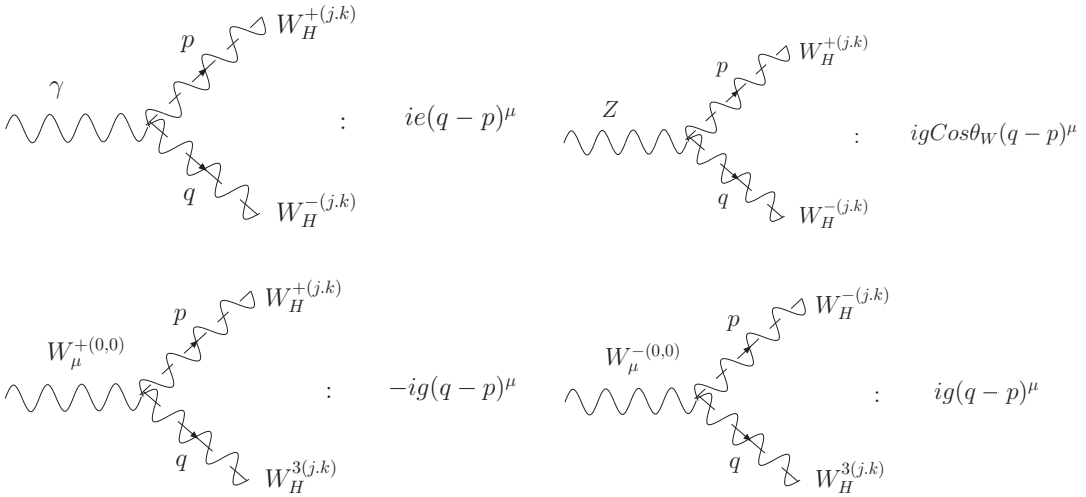

Figure 11: Feynman rules of KK-number conserving interactions of two (j,k)-mode $SU(2)$ spinless adjoint ($W_H^{3,\pm(j,k)}$) with a SM vector boson (γ, Z or $W_\mu^{\pm(0,0)}$).

References

[1] I. Antoniadis, Phys. Lett. B **246**, 377 (1990); N. Arkani-Hamed, S. Dimopoulous and G. Dvali, Phys. Lett. B **429**, 263 (1998); I. Antoniadis, N. Arkani-Hamed, S. Dimopoulos and G. R. Dvali, Phys. Lett. B **436**, 257 (1998).

[2] L. Randall and R. Sundrum, Phys. Rev. Lett. **83**, 3370 (1999); *ibid* **83**, 4690 (1999).

[3] A. Donini, S. Rigolin; Nucl. Phys. **B550**, 59 (1999); I. Antoniadis, K. Benakli, M. Quiros; Phys. Lett. B **460**, 176 (1999).

[4] C. Macesanu, C. D. McMullen, S. Nandi; Phys. Rev. D **66**, 015009 (2002);

[5] A. De Rujula , A. Donini, M. B. Gavela, S. Rigolin; Phys. Lett. B **482**, 195 (2000); D. A. Dicus, C. D. McMullen, S. Nandi; Phys. Rev. D **65**, 076007 (2002); C. Macesanu, C. D. McMullen, S. Nandi; Phys. Lett. B **546**, 253 (2002); C. Macesanu , A. Mitov , S. Nandi; Phys. Rev. D **68**, 084008 (2003); C. Macesanu, S. Nandi, C. M. Rujoiu; Phys. Rev. D **73**, 076001 (2006).

[6] T. Appelquist, H. C. Cheng and B. A. Dobrescu, Phys. Rev. D **64**, 035002 (2001); H. C. Cheng, K. T. Matchev and M. Schmaltz, Phys. Rev. D **66**, 056006 (2002).

[7] K. Dienes, E. Dudas, T. Gherghetta, Nucl. Phys. **B537**, 47 (1999); K. Dienes, E. Dudas, T. Gherghetta, Phys. Lett. B **436**, 55 (1998); G. Bhattacharyya, A. Datta, S. K. Majee and A. Raychaudhuri, Nucl. Phys. **B760**, 117 (2007).

[8] G. Servant, T. Tait, Nucl. Phys. **B650**, 391 (2003); K. Kong. K. Matchev, J. High Energy Phys. **038**, 0601, (2006).

[9] B. Dobrescu, D. Hooper, K. Kong, R. Mahbubani; Jour. Cosmo. Astro. Phys. **0710**, 012 (2007).

[10] T. Appelquist, B. Dobrescu, E. Ponton, H. Yee, Phys. Rev. Lett. **87**, 181802 (2001).

[11] B. Dobrescu, E. Poppitz, Phys. Rev. Lett. **87**, 031801 (2001).

[12] B. Dobrescu, E. Ponton, J. High Energy Phys. **071**, 0403, (2004).

[13] B. Dobrescu, K. Kong, R. Mahbubani, J. High Energy Phys. **006**, 0707, (2007).

[14] G. Burdman, B. Dobrescu, E. Ponton, Phys. Rev. D **74**, 075008 (2006).

[15] K. Ghosh and A. Datta, Nucl. Phys. **B800**, 109 (2008).

[16] A. Freitas and K. Kong, J. High Energy Phys. **0802**, 068 (2008).

[17] K. Ghosh and A. Datta, Phys. Lett. B **665**, 369 (2008).

[18] E. Ponton, L. Wang, J. High Energy Phys. **018**, 0611, (2006).

[19] C. Amsler *et al.* [Particle Data Group], Phys. Lett. B **667**, 1 (2008).

[20] H. Lai et al., Phys. Rev. D **55**, 1280 (1997).

[21] S. Ambrosanio and B. Mele, Phys. Rev. D **53**, 2541 (1996).

[22] K. Hagiwara and D. Zeppenfeld, Nucl. Phys. **B313**, 560 (1989).